

Photoelectrical properties investigated on individual Si nanowires and their size dependence

X. F. Hu, S. J. Li, Z. M. Jiang, and X. J. Yang*

State Key Laboratory of Surface Physics, Fudan University, Shanghai 200433, China

Periodically ordered arrays of vertically aligned Si nanowires (Si NWs) are successfully fabricated with controllable diameters and lengths. Their photoconductive properties are investigated by photoconductive atomic force microscopy (PCAFM) on individual nanowires. The results show that the photocurrent of Si NWs increases significantly with the laser intensity, indicating that Si NWs have good photoconductance and photoresponse capability. This photo-enhanced conductance can be attributed to the photo-induced Schottky barrier change, confirmed by I-V curve analyses. On the other hand, electrostatic force microscopy (EFM) results indicate that a large number of photo-generated charges are trapped in Si NWs under laser irradiation, leading to the lowering of barrier height. Moreover, the size dependence of photoconductive properties is studied on Si NWs with different diameters and lengths. It is found that the increasing magnitude of photocurrent with laser intensity is greatly relevant to the nanowires' diameter and length. Si NWs with smaller diameters and shorter lengths display better photoconductive properties, which agrees well with the size-dependent barrier height variation induced by photo-generated charges. With optimized diameter and length, great photoelectrical properties are achieved on Si NWs. Overall, in this study the photoelectrical properties of individual Si NWs are systematically investigated by PCAFM and EFM, providing important information for the optimization of nanostructures for practical applications.

Keywords: Si nanowires; photoconductive atomic force microscopy; electrostatic force microscopy; photoconductive property; size-dependence

* Corresponding author. E-mail address: xjyang@fudan.edu.cn.

1. Introduction

Silicon nanowires (Si NWs) have attracted great attention in recent years due to their unique properties and compatibility with traditional silicon technology. Si NWs have been demonstrated for a variety of applications, such as integrated logic circuits, solar cells, thermoelectric devices, biosensors, and etc. [1-5]. Particularly, when arranged in a highly ordered way, Si NWs can greatly improve the light absorption and charge collection, making them possible to achieve high efficiency in both solar cells and photodetectors [6-8]. In the past decades, the controllable growth of such ordered nanowire arrays as well as the optimal fabrication of photovoltaic (PV) devices have been intensively investigated [9-11]. Conversely, there are much fewer fundamental studies about the photoelectrical characteristics on such Si NWs arrays, especially on individual nanowires inside the arrays.

In order to realize the applications of ordered nanowire arrays in solar cells and PV devices, it is extremely important to get a good understanding of their photoconductive properties. Nowadays, the photoconductive properties of nanowire arrays are generally investigated by macroscopic methods with the deposition of two-side electrodes under light irradiation [12, 13]. However, for more accurate analysis, it is necessary to achieve the properties on single or individual nanowires rather than averaged results. Besides the studies applying single nanowire devices which is not easy to fabricate, scanning probe microscopy (SPM)-based electrical measurements have revealed themselves as powerful techniques for electrical characterizations at nanoscale [14, 15]. Among these SPM techniques, conductive atomic force microscopy (CAFM) has been most often applied to study the conductive properties of individual nanostructures such as films, heterostructures as well as nanowires [16-20]. By combining with laser irradiation, it can be modified as photoconductive atomic force microscopy (PCAFM) which provides a route to investigate the photoconductive properties on individual nanostructures [21, 22]. In recent years, PCAFM has already been employed to photocurrent measurements on organic [23-26] and inorganic solar cells [27-29], as well as on some nanostructures, including microcrystalline Si thin films, CdS heterostructures, MoS₂ films and ZnO NWs [30-33]. Yet, most of these studies focused on the influence of laser irradiation with varied power intensities or wavelengths, while a few researches concerned with the effect of nanowires' size.

On the other hand, to achieve Si NWs array with excellent photoconductive properties, it is quite necessary to obtain their size dependence for the optimization of nanowires' diameter and length. Hence in recent decades, many efforts have been devoted to revealing the size dependence of photoconductive properties by using macroscopic methods or single nanowire devices [34, 35]. In the aspect of length dependence, many researches found that the photocurrent increased with the increasing of nanowire length below a specific value varied from 1 to 18 μm and then decreased as the length further increased [12, 36, 37], while another study reported that the photoconductance increases sublinearly with decreased length [38]. Meanwhile, the results of diameter dependence were yet much inconsistent. For example, the work by Kim et al. found that photoconductance of intrinsic Ge nanowires increased with the decreased diameter [35], while other works on GaN nanowires found the photocurrent increased as the diameter increased [39]. Therefore, the size dependence of photoconductive properties on nanowires is far from reaching a good and common understanding.

In this paper, ordered arrays of vertically aligned Si NWs with controllable diameters and lengths are successfully fabricated by the method of nanosphere lithography (NSL) combined with metal-assisted chemical etching (MACE), as reported in previous literatures [1, 40]. Their photoconductive properties are investigated by PCAFM without any further nanofabrication. Our results demonstrate that the photocurrent measured on individual Si NWs increases greatly with the laser intensity, and the increasing magnitude is obviously related to the nanowires' size. Si NWs with smaller diameters and shorter lengths are more photoconductive. On the other hand, the measurements performed by electrostatic force microscopy (EFM) combined with laser irradiation provided the information of photo-generated charges and barrier height modification, which can be employed to explain the size-dependent photo-enhanced conductance of Si NWs. Therefore, this study not only reveals the size-dependent photoelectrical properties of Si NWs but also suggests that PCAFM and EFM are effective tools in investigating the photoelectrical properties of individual nanostructures as well as to explore the size (or other parameters) dependence.

2. Materials and Methods

2.1 Materials

The Si wafers were purchased from MTI (China). Deionized water (DI, 18.2 M Ω ·cm) was obtained from an ultrafiltration system (Milli-Q, Millipore, Marlborough, MA). Acetone, methanol, sulphuric acid, hydrogen peroxide, and hydrofluoric acid were purchased from Sinopharm Chemical Reagent (China). The suspensions (2.5 wt% in water) of polystyrene spheres (PS, 490 nm in diameter) were purchased from Duke Scientific (USA).

2.2 Fabrication and characterization of Si NWs

Vertically ordered silicon nanowire arrays were fabricated by NSL and MACE, as reported in previous literatures [1, 40]. The major fabrication processes are simply described as follows. Firstly, polystyrene spheres (PS) were self-assembled onto the chemically cleaned Si wafer (n-type, 0.01-0.02 Ω cm). Next, the diameter of PS spheres was reduced by reactive ion etching (RIE, Trion Technology) (50 W, 70 mTorr) to a desired value, and the diameter-reduced PS monolayer acted as a mask in the following procedures. After a 20 nm Au film deposition by ion sputtering which acted as a catalyst for the following MACE treatment, the sample was dipped in the mixed solution of HF (40%) and H₂O₂ (30%) with a volume ratio of 4:1 for MACE process and vertically aligned Si NWs were produced by this procedure. Finally, the remaining Au layer and PS spheres were removed by soaking the sample in KI/I₂ mixed solution and tetrahydrofuran solution, respectively. The morphology after each step was checked by scanning electron microscopy (SEM, SIGMA300). Typical SEM images of original self-assembled PS monolayer, diameter-reduced PS monolayer and the fabricated Si NWs after removing Au layer and PS spheres were shown in Fig. 1(a), (b) and (c), respectively. It can be seen that ordered arrays of vertically aligned Si NWs were achieved in a large scale. Moreover, by adjusting the RIE and MACE time, the nanowires' diameter and length can be well controlled [40].

The photoelectrical measurements on individual Si NWs were carried out with a commercial SPM

equipment (Multimode V, Bruker Nano Surfaces), as diagramed in Fig. 1(d). In PCAFM, the conductive tip scanned over the sample surface in contact mode with a bias voltage applied between the substrate and electrically grounded tip, and the resulted current was measured. Laser irradiation was introduced into the SPM head through a 400- μm fiber. A 405 nm diode laser with adjustable intensity (DPSS Lasers, MDL-III) was focused onto the substrate, and the laser spot area was about 1 mm^2 beneath the Pt/Cr-coated tip. The intensity of the laser irradiated onto the sample was varied from 0 to 8 W/cm^2 at an interval of 2 W/cm^2 , and the photoconductive currents were measured on individual nanowires. By using EFM, both the sample topography and the electrical force induced phase shift could be recorded by a two-pass mode. In the first pass the topography image was obtained in tapping mode. In the second lifted pass (the tip was lifted high enough to neglect the phase shift induced by van der Waals force), a DC bias was applied between the tip and the sample and the phase shift signal determined by the electrical force gradient was detected. The detailed operation principles could be found in previous literatures [41, 42]. Pt/Cr-coated tips (Multi75E-G, Budget Sensors, radius approximately 25 nm) were applied in all electrical measurements and all experiments were performed in a flowing N_2 ambient. Each sample was pre-dipped in the HF solution (5%) for 30 seconds and measured immediately after HF dipping, in order to reduce the influence of the oxide layer on the electrical characterization as possible.

3. Results and discussions

3.1 Photoconductive property measurements on single Si NWs

By combining with laser irradiation, the photoconductive properties of Si NWs are investigated by PCAFM as a function of laser intensity. Typical current images obtained on the Si NWs with the diameter of 190 nm and length of 800 nm under different laser irradiation at a sample bias of -1.5 V are shown in Fig. 2(b)-(f), together with the topography image shown in Fig. 2(a). Since the tip was a wedge with a large angle making it unable to reach the bottom, especially the images were obtained in contact mode, the observed nanowires are somewhat distorted and only the current on the top side of nanowires can be measured. Anyway the current distribution of individual nanowires can be clearly observed from the current images. In the current image without laser irradiation (Fig. 2(b)), Si NWs exhibit a little better conductance at most of the edges than the center, which was attributed to the larger side contact area between tip and nanowire [40]. Under laser irradiation, the current of Si NWs increases obviously with the laser intensity (Fig. 2(c)-(d)), while the conductive area of nanowires increases correspondingly. To get a distinct relation between photocurrent and laser intensity, the average currents of Si NWs are calculated over all the nanowires in the current maps, which are presented in Fig. 2(g) as a function of laser intensity. The results show that the average current has about two times increase (from 85 to 146 pA) as the laser intensity increases from 0 to 8 W/cm^2 , indicating more carriers are generated under laser irradiation.

In previous literatures [32, 43], photoresponse was usually applied to describe the response capability of photodetectors, which was defined as:

$$R = \frac{(I_L - I_D)/q}{P_{inc}/h\nu}, \quad (1)$$

where I_L and I_D are the current with and without laser irradiation, respectively. P_{inc} is the product of incident laser power density divided by the effective area of the contact area between the tip and the sample, q is the elementary charge and $h\nu$ is the photon energy. In our case the effect contact area is about $2 \times 10^{-11} \text{ cm}^2$ by using the tip radius of 25 nm, and as a result the photoresponse of Si NWs can be calculated to be about 2.3 at the laser intensity of 2 W/cm^2 , indicating that Si NWs have excellent photo enhancement capability. Figure. 2(h) presents the photoresponse as a function of laser intensity, and it can be seen that the photoresponse decreases with the increasing laser intensity but all the values are still larger than 1. Thus the above results demonstrate that the laser irradiation can greatly enhance the conductance of Si NWs, suggesting its promising application potentials in photodetectors.

To investigate the size dependence of the photoconductive properties, photocurrent measurements were performed on the Si NWs with different diameters and lengths. Typical current images of Si NWs with the same length of 350 nm but different diameters from 190 nm to 350 nm are shown in Fig. S1 under 0, 4 and 8 W/cm^2 laser irradiation at the same sample bias of -1.5 V . The average currents of Si NWs calculated over all the nanowires in the current images are presented in Fig. 3(a) as a function of laser intensity. It can be seen that the conductance of Si NWs with all diameters increases obviously with the increased laser intensity. Under the same laser intensity, the absolute current values increase significantly as the diameter decreases from 350 to 190 nm. These results suggest that Si NWs with smaller diameters are more conductive than those with larger ones. The photoresponse averaged over laser intensities is presented in Fig. 3(b) for different diameters. It can be seen that the photoresponse decreases with the increased diameter, which means that Si NWs with smaller diameters have better photoresponse capability. On the other hand, the photocurrent ($I_L - I_D$) at the laser intensity of 8 W/cm^2 for different diameters is shown in Fig. 3(c). It clearly shows that the photocurrent decreases as the diameter increases, indicating that Si NWs with smaller diameters have better photoconductance.

Similar measurements are made on Si NWs with same diameter but different lengths. The results of nanowires with the diameter of 190 nm and lengths from 350 nm to 960 nm are shown in Fig. S2. The average currents of nanowires with different lengths are presented in Fig. 3 (d). With the increased laser intensity, all of the nanowires exhibit an obvious increase in conductance, and the shorter Si NWs have the larger conductance across the laser intensity range up to 8 W/cm^2 . The photoresponse and photocurrent as a function of nanowires' length are presented in Fig. 3(e) and (f), respectively. It can be seen that with the increase of length from 350 to 960 nm, the photoresponse does not show an obvious length dependence, while the photocurrent largely decreases with the increase of length.

3.2 I-V curves analysis and size-dependent Schottky barrier height

As reported in our previous work [40], in CAFM measurements on Si NWs, tip-nanowire contact resistance should be emphatically considered, in which the Schottky barrier plays an important role. To investigate the role of Schottky barrier in photoconductance and the effect of laser irradiation on barrier height,

current-voltage (I-V) curves are recorded on individual Si NWs. Typical I-V curves on the Si NWs with the diameter of 190 nm and length of 800 nm under different laser irradiation are presented in Fig. 4(a). All the I-V curves exhibit typical I-V characteristic of metal and n-type semiconductor contact, indicating the effect of oxygen layer on conductance is not serious and thus ignored in the following discussion. It can be observed that, as the laser intensity increases, the current of the Si NWs increases obviously. The enhancement can reach about 3 times when the laser intensity increases from 0 to 8 W/cm² under the bias of -1.5 V, which is well consistent with the results obtained from current images. To get a quantitative analysis, a well-known thermionic emission model for a metal-semiconductor contact is adopted [13, 44]. In this model, the I-V characteristics of a Schottky contact to n-type semiconductor in the presence of series resistance can be approximated as [13]:

$$I = I_s \left[\exp\left(\frac{q(V - IR_s)}{nkT}\right) - 1 \right], \quad (2)$$

where n is the ideal factor and R_s is the series resistance. I_s is the saturation current, which can be expressed by:

$$I_s = AA^* T^2 \exp\left(-\frac{\phi_B}{kT}\right), \quad (3)$$

where A is the contact area, A^* is Richardson's constant, and ϕ_B is the Schottky barrier height (SBH) between the metal tip and Si nanowire. Thus, SBH can be obtained with the formula:

$$\phi_B = kT \ln\left(\frac{AA^* T^2}{I_s}\right), \quad (4)$$

The I-V curves in Fig. 4(a) can be well fitted by equation (2). To get the SBH values from the saturation current, the effective Richardson constant A^* is assumed to be approximately equal to that of bulk silicon, i.e. 112 A cm⁻² K⁻² for n-type silicon. The contact area is assumed to be 2×10⁻¹¹ cm² by taking the Cr/Pt coated tip radius as 25 nm. The SBH values are obtained to be about 474, 453, 437, 429 and 416 meV for different laser intensities of 0, 2, 4, 6 and 8 W/cm², respectively, as plotted in Fig. 4 (b). It demonstrates that SBH decreases significantly with the laser intensity, which may be the main contributor to the photo-enhanced conductance. At the meantime, the dependence of SBH on the nanowires' diameter and length at the same laser intensity is given in Fig. 4 (c) and (d), respectively. The results indicate that Si NWs with smaller diameters and shorter lengths have smaller SBH values, resulting in better photoconductance obtained on such nanowires. The diameter and length dependence of SBH under different laser irradiation are shown in Fig. S3, which further supports the above conclusion. Obviously, all of the measured SBH values for Si NWs with different diameters and lengths are smaller than that of the bulk Si (~600 meV) [40] and further decrease with the increased laser intensity, indicating that Si NWs can achieve promising photoconductive properties for potential applications.

3.3 Photo-generated trapped charges and barrier height modification

To further verify the SBH results of Si NWs obtained by PCAFM, EFM images were measured on Si NWs under different laser irradiation, as shown in Fig. 5 (a)-(d). It can be seen that the electrostatic force induced phase shift ($\Delta\phi$) increases obviously with the laser intensity. The phase shift image acquired in line scan mode on the top center of the nanowire is presented in Fig. 5(e), and the averaged phase shift over the scan line along

the marked curve is drawn in Fig. 5 (f). Both of them clearly exhibit the increase of $\Delta\Phi$ with laser intensity.

To get more definite information from EFM measurements, $\Delta\Phi$ was measured as a function of applied voltage (V_{EFM}) under different laser irradiation on a certain single nanowire. A set of $\Delta\Phi \sim V_{EFM}$ curves measured on the Si nanowire with the diameter of 190 nm and the length of 800 nm are presented in Fig.5 (a) as the scattered dots. It can be seen that, with the increase of laser intensity, the $\Delta\Phi \sim V_{EFM}$ curves shift downward. It indicates more carriers are generated and trapped in nanowires [42]. For quantitative analysis, the tip-sample system is simply treated as a plane capacitor, and the capacitive electrostatic force gradient would cause a phase shift when applying a bias between the tip and sample. With charges trapped in the nanostructures by laser irradiation, additional phase shift induced by the Coulombic force would be generated [45]. The phase shift detected by EFM can be described as [46-47]:

$$\Delta\Phi = -\frac{Q}{k} \frac{\partial F}{\partial z} = -\frac{Q}{k} \left[\frac{1}{2} \frac{\partial^2 C}{\partial z^2} (V_{EFM} - V_{CPD})^2 + \frac{Q_s}{2\pi\epsilon_0 z^2} \left(\frac{C}{z} - \frac{1}{2} \frac{\partial C}{\partial z} \right) (V_{EFM} - V_{CPD}) + \frac{Q_s^2}{2\pi\epsilon_0 z^3} \right], \quad (5)$$

where C , V_{EFM} and V_{CPD} are the capacitance, applied DC voltage and contact potential difference between the tip and sample, respectively. Q_s is the quantity of charges trapped in the nanowire, Q is the quality factor and k is the spring constant of the probe, and z is the distance between the trapped charges in nanowire.

$\Delta\Phi \sim V_{EFM}$ curves in Fig. 5 (a) can be well fitted by using equation (5), shown as the solid lines. From the fitting parameters, V_{CPD} and Q_s can be obtained using $Q = 186$ and $k = 2.8$ N/m for Pt/Ir-coated tip [48, 49] and approximating z as the lift height, which are plotted in Fig. 5 (b) as a function of laser intensity. It can be seen that, with the increase of laser intensity, V_{CPD} decreases while the trapped charges Q_s increase. As reported in literature [42], the change of V_{CPD} under laser irradiation was related to the variation in trapped carrier density. Thus the decrease of V_{CPD} with laser irradiation in our experiments can also be attributed to the increase of trapped charge density.

From the energy diagram given in Fig. S4, the value of SBH roughly equals to qV_{CPD} plus $E_n (= E_C - E_F)$ [40]. As E_n is a constant for all Si NWs made from the same material, the size dependence of V_{CPD} well represents that of SBH. The results of V_{CPD} obtained on Si NWs with different diameters and lengths are presented in Fig. S5 as a function of laser intensity. All of the measured V_{CPD} for Si NWs with different diameters and lengths decrease with the increased laser intensity. The dependence of V_{CPD} on nanowires' diameter and length at the same laser intensity of 8 W/cm² is shown in Fig. 5 (c) and (d), respectively. It can be seen that the V_{CPD} increases obviously with the increased diameter and increased length, in a good agreement with the size dependence of SBH. Therefore, from the EFM results, it can be suggested the laser irradiation can generate carriers trapped in nanowires, which can induce the lowering of barrier height leading to the enhancement of conductance.

4. Conclusion

In summary, by a simple and low-cost method without involving any intricate procedures, Si NWs arrays with controllable diameters and lengths are prepared. The photoconductive properties are directly measured on individual Si NWs without complex nanofabrication procedure by the means of PCAFM. The size-dependent conductance of Si NWs is obtained on individual nanowires with different diameters and lengths.

The results demonstrate that the photocurrent measured on individual Si NWs increases greatly with the laser intensity, and the increasing magnitude is obviously related to the nanowires' sizes. Si NWs with smaller diameters and shorter lengths exhibit larger photoconductance. On the other hand, the measurements performed by EFM combined with laser irradiation provided the information of photo-generated charges and contact barrier height, which can be applied to explain the photoconductive properties of Si NWs as well as their size-dependence. Therefore in this study, the photoelectrical properties are investigated on individual nanowires by PCAFM and EFM, which should be important for both basic understanding and potential applications of nanostructures in optoelectronics and photovoltaics.

Abbreviations

Si NWs: Si nanowires; CAFM: conductive atomic force microscopy; PCAFM: photoconductive conductive atomic force microscopy; EFM: electrostatic force microscopy; PV: photovoltaic; NSL: nanosphere lithography; MACE: metal-assisted chemical etching; SPM: scanning probe microscopy; PS: polystyrene spheres; RIE: reactive ion etching; SEM: scanning electron microscopy; SBH: Schottky barrier height; CPD: contact potential difference.

Acknowledgements

The RIE experiments were carried out in Fudan Nanofabrication Laboratory.

Authors' contributions

XFH carried out the experiments. XFH and XJY interpreted the results and wrote the manuscript. SJL and ZMJ helped in interpretation and discussions. All authors read and approved the final manuscript.

Funding

This work was supported by the Natural Science Foundation of Shanghai (No. 17ZR1402600).

Availability of data and materials

The datasets used for supporting the conclusion are included in the article and the supporting file.

Competing interests

The authors declare that they have no competing interests.

References

1. Lin D, Wu Z, Li S, Zhao W, Ma C, Wang J, Jiang Z, Zhong Z, Zheng Y and Yang X (2017) Large-area Au-nanoparticle-functionalized Si nanorod arrays for spatially uniform surface-enhanced Raman spectroscopy. *ACS Nano* 11 (2):1478
2. Lard M, Linke H and Prinz C N (2019) Biosensing using arrays of vertical semiconductor nanowires: mechanosensing and biomarker detection. *Nanotechnology* 30 (21):214003
3. Fukata N, Subramani T, Jevasuwan W, Dutta M and Bando Y (2017) Functionalization of silicon nanostructures for energy-related applications. *Small* 13 (45): 1701713
4. Yang P, Yan R and Fardy M (2010) Semiconductor nanowire: what's next? *Nano Lett* 10 (5):1529
5. Su X, Wu Q, Li J, Xiao X, Lott A, Lu W, Sheldon B W and Wu J (2014) Silicon-based nanomaterials for lithium-ion batteries: A review. *Adv Energy Mater* 4 (1):1300882
6. Long Y-Z, Yu M, Sun B, Gu C-Z and Fan Z (2012) Recent advances in large-scale assembly of semiconducting inorganic nanowires and nanofibers for electronics, sensors and photovoltaics. *Chem Soc Rev* 41 (12):4560
7. Tsakalakos L (2008) Nanostructures for photovoltaics. *Mat Sci Eng R* 62 (6):175
8. Soci C, Zhang A, Bao X-Y, Kim H, Lo Y and Wang D (2010) Nanowire photodetectors. *J Nanosci Nanotech* 10 (3):1430
9. Peng K-Q, Wang X, Li L, Hu Y and Lee S-T (2013) Silicon nanowires for advanced energy conversion and storage. *Nano Today* 8 (1):75
10. Wang Y, Wang T, Da P, Xu M, Wu H and Zheng G (2013) Silicon nanowires for biosensing, energy storage, and conversion. *Adv Mater* 25 (37):5177
11. LaPierre R R, Chia A C E, Gibson S J, Haapamaki C M, Boulanger J, Yee R, Kuyanov P, Zhang J, Tajik N, Jewell N and Rahman K M A (2013) III-V nanowire photovoltaics: Review of design for high efficiency. *Phys Status Solidi-R* 7 (10):815
12. Yuan G, Zhao H, Liu X, Hasanali Z S, Zou Y, Levine A and Wang D (2009) Synthesis and photoelectrochemical study of vertically aligned silicon nanowire arrays. *Angew Chem Int Ed Engl* 48 (51):9680
13. Yang Z, Du K, Wang H, Lu F, Pang Y, Wang J, Gan X, Zhang W, Mei T and Chua S J (2019) Near-infrared photodetection with plasmon-induced hot electrons using silicon nanopillar array structure. *Nanotechnology* 30 (7):075204
14. Giridharagopa R, Shao G, Groves C and Ginger D S (2010) New SPM techniques for analyzing OPV materials. *Mater Today* 13 (9):50
15. Hui F and Lanza M (2019) Scanning probe microscopy for advanced nanoelectronics. *Nat Electron* 2 (6):221
16. Liu J, Goswami A, Jiang K, Khan F, Kim S, McGee R, Li Z, Hu Z, Lee J and Thundat T (2018) Direct-current triboelectricity generation by a sliding Schottky nanocontact on MoS₂ multilayers. *Nat Nanotechnol* 13 (2):112
17. Yang T, Hertenberger S, Morkötter S, Abstreiter G and Koblmüller G (2012) Size, composition, and doping effects on In(Ga)As nanowire/Si tunnel diodes probed by conductive atomic force microscopy. *Appl Phys Lett* 101 (23): 233102
18. Tang C, Jiang C, Bi S and Song J (2016) Photoelectric property modulation by nanoconfinement in the longitude direction of short semiconducting nanorods. *ACS Appl Mater Interfaces* 8 (17):11001
19. Alvarez J, Ngo I, Gueunier-Farret M E, Kleider J P, Yu L, Cabarrocas P R, Perraud S, Rouviere E, Celle C, Mouchet C and Simonato J P (2011) Conductive-probe atomic force microscopy characterization of silicon nanowire. *Nanoscale Res Lett* 6 (1):110
20. Xia H, Lu Z-Y, Li T-X, Parkinson P, Liao Z-M, Liu F-H, Lu W, Hu W-D, Chen P-P, Xu H-Y, Zou J and Jagadish C (2012) Distinct photocurrent response of individual GaAs nanowires induced by n-type doping. *ACS Nano* 6 (7):6005
21. O'Dea J R, Brown L M, Hoepker N, Marohn J A and Sadewasser S (2012) Scanning probe microscopy of solar cells: From inorganic thin films to organic photovoltaics. *MRS Bulletin* 37 (7):642
22. Dang X-D, Tamayo A B, Seo J, Hoven C V, Walker B and Nguyen T-Q (2010) Nanostructure and optoelectronic characterization of small molecule bulk heterojunction solar cells by photoconductive atomic force microscopy. *Adv Funct Mater* 20 (19):3314
23. Guide M, Dang X D and Nguyen T Q (2011) Nanoscale characterization of tetrabenzoporphyrin and fullerene-based solar cells by photoconductive atomic force microscopy. *Adv Mater* 23 (20):2313

24. Coffey D C, Reid O G, Deanna B, Rodovsky, Bartholomew G P and Ginger D S (2007) Mapping local photocurrents in polymerfullerene solar cells with photoconductive atomic force microscopy. *Nano Lett* 7 (3):738
25. Hamadani B H, Jung S, Haney P M, Richter L J and Zhitenev N B (2010) Origin of nanoscale variations in photoresponse of an organic solar cell. *Nano Lett* 10 (5):1611
26. Kamkar D A, Wang M, Wudl F and Nguyen T-Q (2012) Single nanowire OPV properties of a fullerene-capped P3HT dyad investigated using conductive and photoconductive AFM. *ACS Nano* 6 (2):1149
27. Heo J-H (2012) Characterization of photoinduced current in poly-Si solar cell by employing photoconductive atomic force microscopy (PC-AFM). *Trans Electr Electron Mater* 13 (1):35
28. Heo J (2013) Characterization of wavelength effect on photovoltaic property of poly-Si solar cell using photoconductive atomic force microscopy (PC-AFM). *Trans Electr Electron Mater* 14 (3):160
29. Zhao Z, Chen X, Wu H, Wu X and Cao G (2016) Probing the photovoltage and photocurrent in perovskite solar cells with nanoscale resolution. *Adv Funct Mater* 26 (18):3048
30. Ledinský M, Fejfar A, Vetushka A, Stuchlík J, Rezek B and Kočka J (2011) Local photoconductivity of microcrystalline silicon thin films measured by conductive atomic force microscopy. *Phys Status Solidi-R* 5 (10-11):373
31. Li Z, Li H, Jiang K, Ding D, Li J, Ma C, Jiang S, Wang Y, Anthopoulos T D and Shi Y (2019) Self-powered perovskite/CdS heterostructure photodetectors. *ACS Appl Mater Interfaces* 11 (43):40204
32. Son Y, Wang Q H, Paulson J A, Shih C-J, Rajan A G, Tvrđy K, Kim S, Alfeeli B, Braatz R D and Strano M S (2015) Layer number dependence of MoS₂ photoconductivity using photocurrent spectral atomic force microscopic imaging. *ACS Nano* 9 (3):2843
33. Fan Z, Dutta D, Chien C-J, Chen H-Y, Brown E C, Chang P-C and Lu J G (2006) Electrical and photoconductive properties of vertical ZnO nanowires in high density arrays. *Appl Phys Lett* 89 (21): 213110
34. Sanford N A, Robins L H, Blanchard P T, Soria K, Klein B, Eller B S, Bertness K A, Schlager J B and Sanders A W (2013) Studies of photoconductivity and field effect transistor behavior in examining drift mobility, surface depletion, and transient effects in Si-doped GaN nanowires in vacuum and air. *J Appl Phys* 113 (17):174306
35. Kim C J, Lee H S, Cho Y J, Kang K and Jo M H (2010) Diameter-dependent internal gain in ohmic Ge nanowire photodetectors. *Nano Lett* 10 (6):2043
36. Wu S, Yu H, Lu N, Quan X and Chen S (2017) Fabrication of the hierarchical structure photocathode by structuring the surface nanopores on Si nanowires standing on p-Si wafer for the effective photoelectrochemical reduction of Cr(VI) in the aqueous solution. *Sep Purif Technol* 175 454
37. Wu S L, Wen L, Cheng G A, Zheng R T and Wu X L (2013) Surface morphology-dependent photoelectrochemical properties of one-dimensional Si nanostructure arrays prepared by chemical etching. *ACS Appl Mater Inter* 5 (11):4769
38. Dong F, Chu V and Conde J P (2011) Submicron thin-film amorphous silicon photoconductive light sensors. *Senser Actuat A-Phys* 170 (1-2):32
39. Calarco R and Marso M (2005) Size-dependent photoconductivity in MBE-grown GaN-nanowires. *Nano Lett* 5 (5):981
40. Hu X F, Li S J, Wang J, Jiang Z M and Yang X J (2020) Investigating size-dependent conductive properties on individual Si nanowires. *Nanoscale Res Lett* 15 (1):52
41. Altvater M A, Wu S, Zhang Z, Zhu T, Li G, Watanabe K, Taniguchi T and Andrei E Y (2019) Electrostatic imaging of encapsulated graphene 2D Mater 6 (4): 045034
42. Wu S, Wu Z, Lin D, Zhong Z, Jiang Z and Yang X (2014) Photogenerated charges and surface potential variations investigated on single Si nanorods by electrostatic force microscopy combined with laser irradiation. *Nanoscale Res Lett* 9 (1):245
43. Son Y, Li M-Y, Cheng C-C, Wei K-H, Liu P, Wang Q H, Li L-J and Strano M S (2016) Observation of switchable photoresponse of a monolayer WSe₂-MoS₂ lateral heterostructure via photocurrent spectral atomic force microscopic imaging. *Nano Lett* 16 (6):3571
44. Park J Y, Lee H, Renzas J R, Zhang Y and Somorjai G A (2008) Probing hot electron flow generated on Pt nanoparticles with Au TiO₂ Schottky diodes during catalytic CO oxidation. *Nano Lett* 8 (8):2388
45. Dokukin M, Olac-Vaw R, Guz N, Mitin V and Sokolov I (2009) Addressable photocharging of single quantum dots assisted with atomic force microscopy probe. *Appl Phys Lett* 95 (17): 173105
46. Lei C H, Das A, Elliott M and Macdonald J E (2004) Quantitative electrostatic force microscopy-phase measurements. *Nanotechnology* 15 (5):627

47. Jespersen T S and Nygård J (2005) Charge trapping in carbon nanotube loops demonstrated by electrostatic force microscopy. *Nano Lett* 8 (9):1838
48. Yalcin S E, Labastide J A, Sowle D L and Barnes M D (2011) Spectral properties of multiply charged semiconductor quantum dots. *Nano Lett* 11 (10):4425
49. Yalcin S E, Yang B, Labastide J A and Barnes M D (2012) Electrostatic force microscopy and spectral studies of electron attachment to single quantum dots on indium tin oxide substrates. *J Phys Chem C* 116 (29):15847

Figure captions

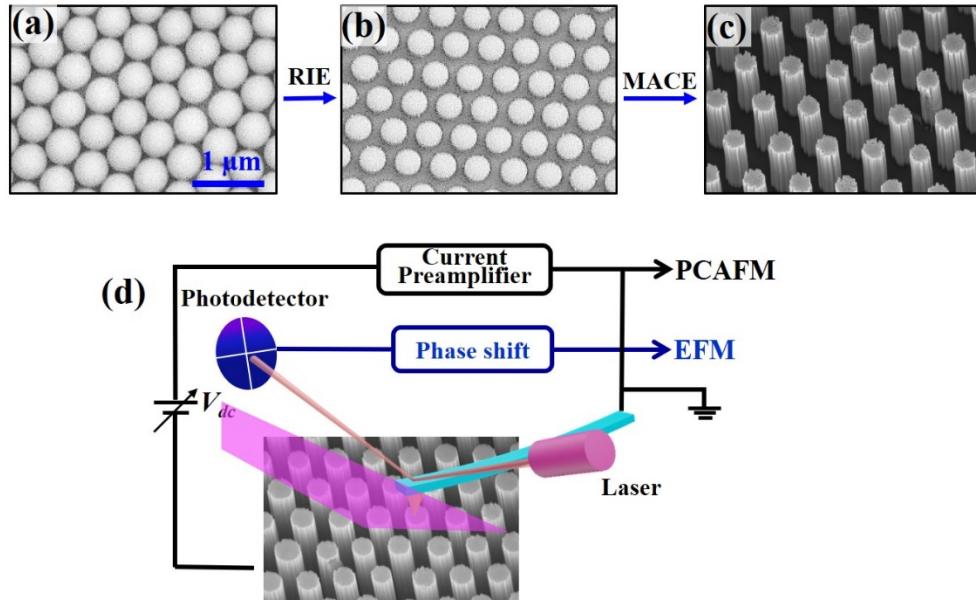


Fig. 1 (a)-(c) SEM images of main procedures to fabricate vertically aligned Si NWs array: (a) Self-assembled PS monolayer, (b) diameter-reduced PS monolayer and (c) fabricated Si NWs array. (d) Schematic diagrams of PCAFM and EFM under laser irradiation.

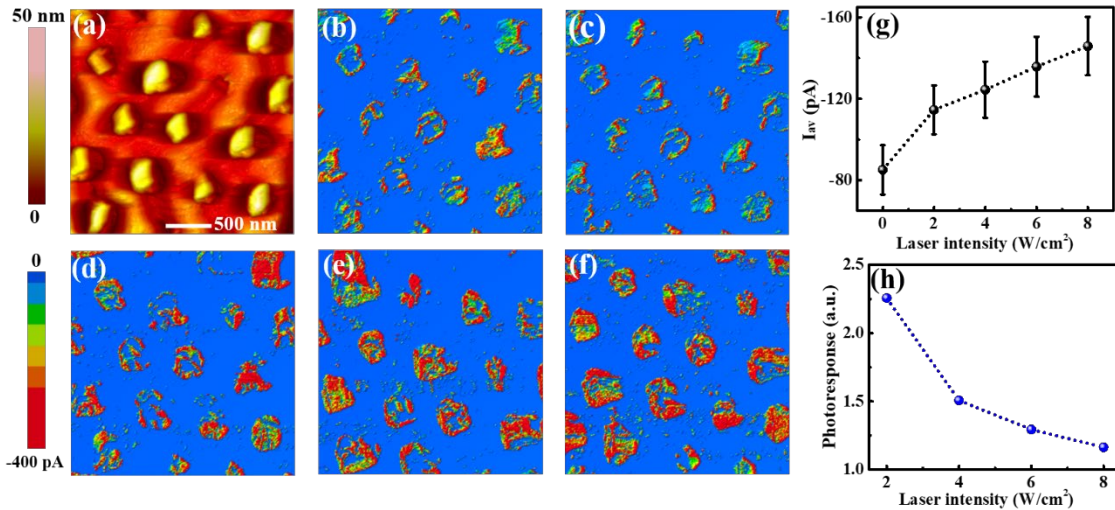


Fig. 2 The topography (a) and current images of Si NWs with the length of 800 nm and diameter of 190 nm under different laser intensities of (b) 0, (c) 2, (d) 4, (e) 6 and (f) 8 W/cm². (g) presents the averaged current (I_{av}) over the nanowires as a function of laser intensity. (h) shows the photoresponse as a function of laser intensity.

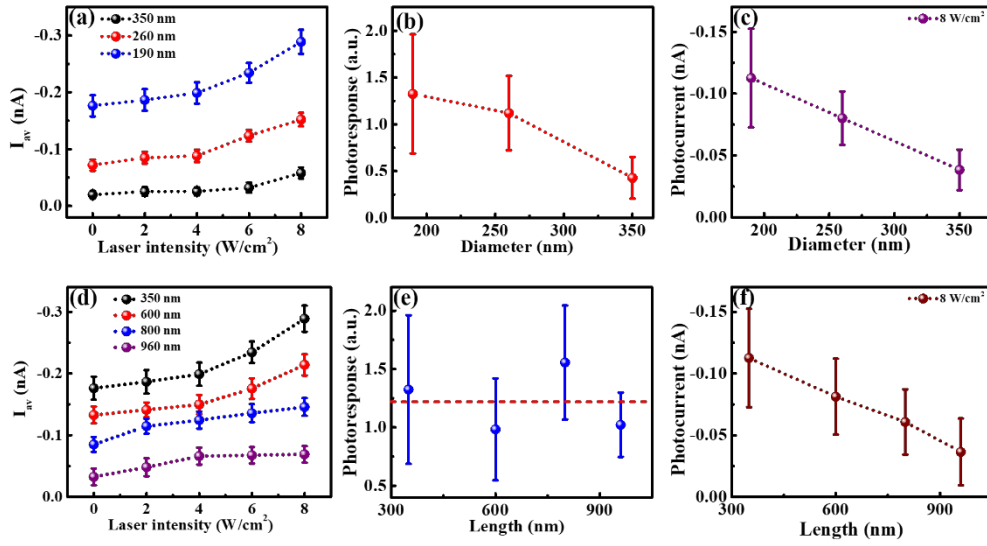


Fig. 3 (a) The averaged current (I_{av}) of Si NWs with different diameters as a function of laser intensity. (b) The averaged photoresponse over the laser intensities as a function of diameters. (c) The dependence of photocurrent on diameter at the laser intensity of 8 W/cm². (d) The I_{av} of Si NWs with different lengths as a function of laser intensity. (e) The averaged photoresponse over the laser intensities as a function of length. (f) The dependence of photocurrent on length at the laser intensity of 8 W/cm².

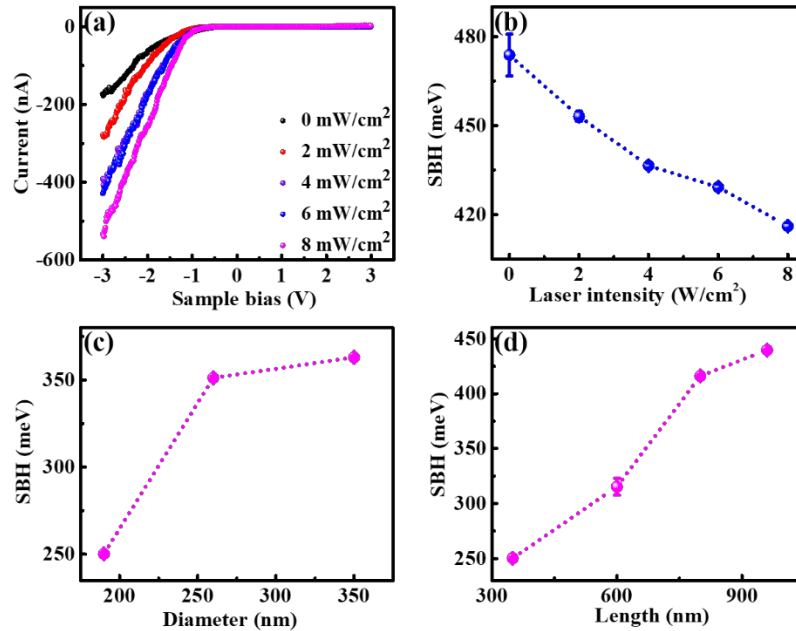


Fig. 4 (a) Typical I-V curves of Si NWs with 190 nm in diameter and 800 nm in length under different laser irradiation. (b) SBH values obtained from the fitting of I-V curves in (a). The diameter- and length-dependent SBH values under 8 W/cm² laser irradiation are plotted in (c) and (d), respectively.

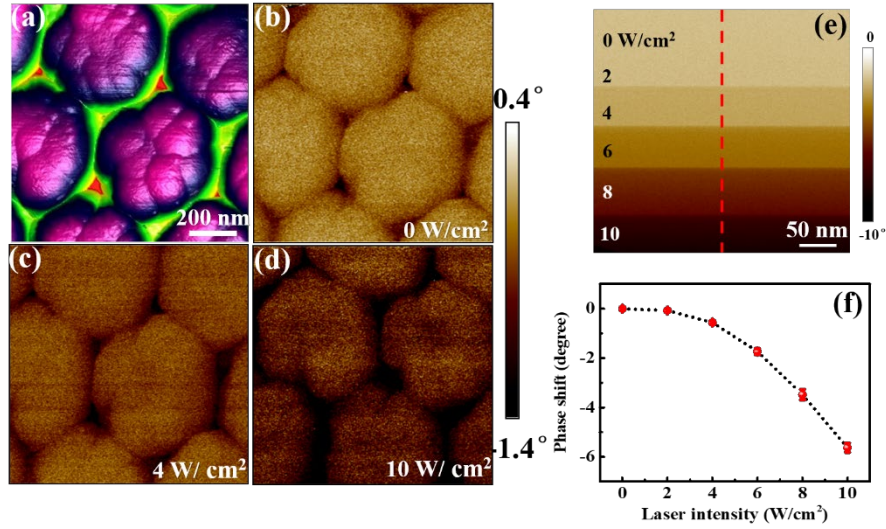


Fig. 5 The topography image of Si NWs (a), the phase shift images obtained at different laser intensities of 0 (b), 4 (c) and 10 W/cm² (d), respectively. (e) The phase shift image acquired in line scan mode on the top center of nanowire. The averaged phase shift over the scan line along the marked red curve in (e) is plotted in (f).

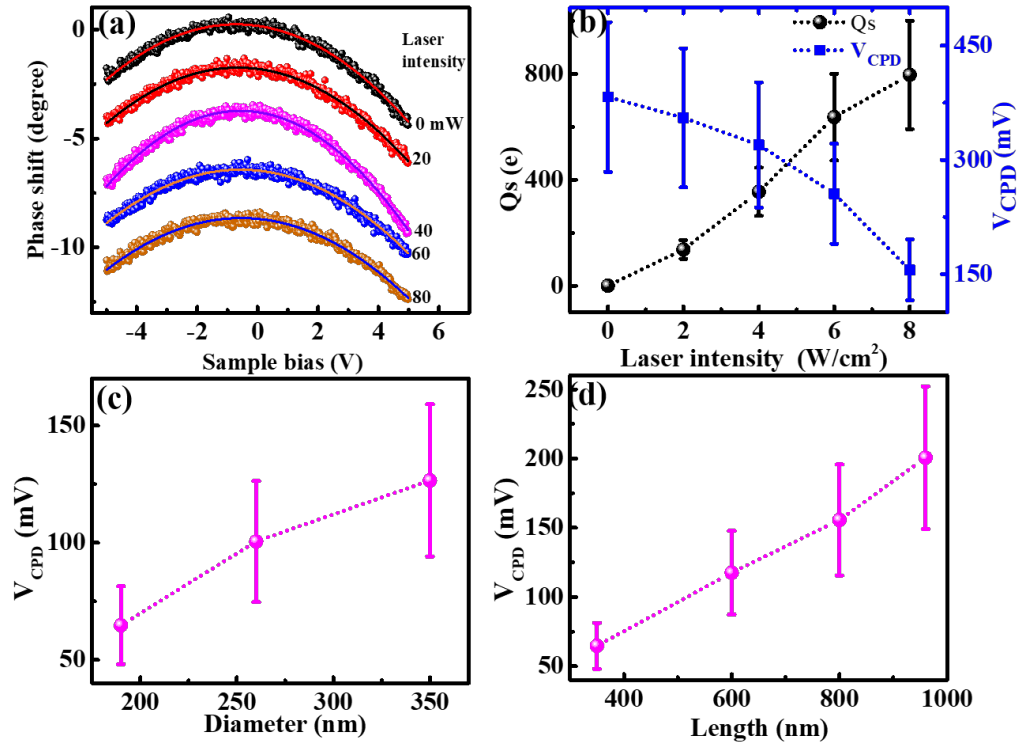


Fig. 6 (a) $\Delta\Phi \sim V_{EFM}$ curves measured by EFM on individual Si NWs with the diameter of 190 nm and length of 800 nm under different laser irradiation. (b) The results of Q_s and V_{CPD} obtained by fitting the curves in (a) as a function of laser intensity. The diameter and length dependence of V_{CPD} at the laser intensity of 8 W/cm² is presented in (c) and (d), respectively.